ornl

OAK RIDGE NATIONAL LABORATORY

MARTIN MARIETTA

ORNL/TM-13066

RECEIVED
FEB 27 1996
OSTI

Fuel Loading and Homogeneity Analysis of HFIR Design Fuel Plates Loaded with Uranium Silicide Fuel

P. E. Blumenfeld

August 1995

Advanced Neutron Source

DISTRIBUTION OF THIS DOCUMENT IS UNLIMITED

MANAGED BY
MARTIN MARIETTA ENERGY SYSTEMS, INC.
FOR THE UNITED STATES
DEPARTMENT OF ENERGY

MASTER

This report has been reproduced directly from the best available copy.

Available to DOE and DOE contractors from the Office of Scientific and Technical Information, P.O. Box 62, Oak Ridge, TN 37831; prices available from (615) 576-8401, FTS 626-8401.

Available to the public from the National Technical Information Service, U.S. Department of Commerce, 5285 Port Royal Rd., Springfield, VA 22161.

This report was prepared as an account of work sponsored by an agency of the United States Government. Neither the United States Government nor any agency thereof, nor any of their employees, makes any warranty, express or implied, or assumes any legal liability or responsibility for the accuracy, completeness, or usefulness of any information, apparatus, product, or process disclosed, or represents that its use would not infringe privately owned rights. Reference herein to any specific commercial product, process, or service by trade name, trademark, manufacturer, or otherwise, does not necessarily constitute or imply its endorsement, recommendation, or favoring by the United States Government or any agency thereof. The views and opinions of authors expressed herein do not necessarily state or reflect those of the United States Government or any agency thereof.

ORNL/TM-13066

FUEL LOADING AND HOMOGENEITY ANALYSIS OF HFIR DESIGN FUEL PLATES LOADED WITH URANIUM SILICIDE FUEL

P. E. Blumenfeld

Date Published: August 1995

Prepared by
OAK RIDGE NATIONAL LABORATORY
Oak Ridge, Tennessee 37831
managed by
LOCKHEED MARTIN ENERGY SYSTEMS, INC.
for the
U.S. DEPARTMENT OF ENERGY
under contract DE-AC05-84OR21400

CONTENTS

LIST OF FIGURES v

LIST OF TABLES vii

ACRONYMS ix

ABSTRACT xi

1. INTRODUCTION 1-1
   1.1 ADVANCE NEUTRON SOURCE BACKGROUND 1-1
   1.2 STATISTICAL EVALUATION OF THERMAL-HYDRAULIC UNCERTAINTIES . . . 1-1
   1.3 IMPORTANCE OF FUEL LOADING PARAMETERS 1-1
   1.4 PREVIOUS ESTIMATES OF FUEL LOADING STATISTICS 1-1
   1.5 THE PRESENT ANALYSIS BASED ON DETAILED DATA 1-2

2. FUEL LOADING MEASUREMENT 2-1
   2.1 FUEL PLATE DESCRIPTION 2-1
   2.2 X-RAY ATTENUATION SCANNING 2-1

3. REFERENCE STANDARDS 3-1
   3.1 STANDARDS WIDTH 3-1
   3.2 EXTRAPOLATING STANDARDS DATA 3-1

4. CONVERSION OF COUNTS TO PERCENT DEVIATION 4-1

5. OVERALL PERCENT DEVIATION 5-1
   5.1 IMPACT OF SILICIDE FUEL ON HOMOGENEITY SCAN DATA 5-2
   5.2 CONVERTING OXIDE REFERENCED SCAN DATA FOR SILICIDE FUEL USING OVERALL PERCENT DEVIATION 5-3

6. STATISTICAL ANALYSIS OF FUEL PLATES 6-1
   6.1 ISOLATING THE FUELED REGION 6-1
   6.2 LOCAL ANALYSIS 6-2
   6.3 χ^2 TEST FOR NORMAL DISTRIBUTIONS 6-2
      6.3.1 Observed Frequencies 6-3
      6.3.2 Normal Probabilities and Expected Frequencies 6-3
      6.3.3 Interpreting χ^2 Test Results 6-4
   6.4 LOCAL ANALYSIS RESULTS 6-4
   6.5 HOT SEGMENT ANALYSIS 6-4
   6.6 HOT SEGMENT ANALYSIS RESULTS 6-6
   6.7 HOT STREAK ANALYSIS 6-8
   6.8 HOT STREAK ANALYSIS RESULTS 6-8

7. CONCLUSIONS 7-1

8. SUGGESTIONS FOR FUTURE WORK 8-1

9. REFERENCES 9-1

APPENDIX A. DETERMINATION OF RELATIVE THICKNESS FOR USE IN OVERALL PERCENT DEVIATION CALCULATION A-1

APPENDIX B. MANUFACTURING DATA FOR URANIUM SILICIDE LOADED FUEL PLATES B-1

APPENDIX C. ASSUMPTIONS REQUIRED FOR OXIDE TO SILICIDE PERCENT DEVIATION CONVERSION C-1

LIST OF FIGURES

Figure		Page
2.1	Homogeneity scanner setup	2-2
2.2	Counts data plotted as a function of track and position	2-2
3.1	Closeup of counts data in standards region	3-2
4.1	Uncorrected oxide and silicide homogeneity scans (PD)	4-2
4.2	Guide to image features	4-3
5.1	Corrected oxide and silicide homogeneity scans (CPD)	5-5
6.1	Scan data for fueled region	6-1
6.2	Local CPD distributions	6-5
6.3	Hot segment CPD distributions	6-7
6.4	Hot streak CPD distributions	6-10
A.1	Radial contour of HFIR fuel plates	A-2
A.2	Counts vs relative thickness with track 0 set at 0.00 mm	A-4
A.3	Counts vs relative thickness with track 0 set at −1.19 mm	A-4
C.1	Material thickness correlations for equal attenuations	C-3
C.2	Observed U_3O_8 and hypothetical U_3Si_2 fuel meat thickness correlated with aluminum thickness	C-4

LIST OF TABLES

Table		Page
5.1	Effect of fuel mass and uranium loading on overall percent deviation	5-2
6.1	Local analysis results	6-6
6.2	Hot segment analysis results	6-8
6.3	Hot streak analysis results	6-9

ACRONYMS

ANS	Advance Neutron Source
CPD	corrected percent deviation
HFIR	High Flux Isotope Reactor
OPD	overall percent deviation
PD	percent deviation
TASHA	Thermal Analysis of Steady state Heat transfer for ANS (computer code)

ABSTRACT

Twelve nuclear reactor fuel plates were analyzed for fuel loading and fuel loading homogeneity by measuring the attenuation of a collimated X-ray beam as it passed through the plates. The plates were identical to those used by the High Flux Isotope Reactor (HFIR) but were loaded with uranium silicide rather than with HFIR's uranium oxide fuel. Systematic deviations from nominal fuel loading were observed as higher loading near the center of the plates and underloading near the radial edges. These deviations were within those allowed by HFIR specifications.

The report begins with a brief background on the thermal-hydraulic uncertainty analysis for the Advanced Neutron Source (ANS) Reactor that motivated a statistical description of fuel loading and homogeneity. The body of the report addresses the homogeneity measurement techniques employed, the numerical correction required to account for a difference in fuel types, and the statistical analysis of the resulting data. This statistical analysis pertains to local variation in fuel loading, as well as to "hot segment" analysis of narrow axial regions along the plate and "hot streak" analysis, the cumulative effect of hot segment loading variation.

The data for all twelve plates were compiled and divided into 20 regions for analysis, with each region represented by a mean and a standard deviation to report percent deviation from nominal fuel loading. The central regions of the plates showed mean values of about +3% deviation, while the edge regions showed mean values of about –7% deviation. The data within these regions roughly approximated random samplings from normal distributions, although the chi-square (χ^2) test for goodness of fit to normal distributions was not satisfied.

1. INTRODUCTION

1.1 ADVANCE NEUTRON SOURCE BACKGROUND

The ANS is a proposed new facility intended to provide its users with the world's most intense steady state neutron beams.[1] The source of neutrons is a research reactor, and to achieve the required neutron fluxes, the ANS reactor must operate with a high thermal power density and peak heat flux. The ANS thermal-hydraulic design team is presented with the task of removing 4.5 MW of thermal power from each liter of core volume. The feasibility of this goal cannot be established if overly conservative "worst-case" values are assumed when evaluating uncertainties in the reactor core design.

1.2 STATISTICAL EVALUATION OF THERMAL-HYDRAULIC UNCERTAINTIES

A statistical/probabilistic approach to the uncertainty analysis has been adopted to avoid an overly conservative or restrictive design. It is intended to determine maximum power operating limits while maintaining acceptable safety margins.[2] The statistical/probabilistic approach has been implemented through a Monte Carlo sampling technique. The Monte Carlo routine sets values for various thermal-hydraulic input parameters for a simulation code called TASHA (Thermal Analysis of Steady state Heat transfer for ANS).[3] As the TASHA code is run repeatedly using values sampled randomly from known distributions for the input parameters, the results point to a maximum power operating level that will satisfy probabilistic risk requirements.

1.3 IMPORTANCE OF FUEL LOADING PARAMETERS

A sensitivity check was made using the TASHA code to determine the relative importance of the many thermal-hydraulic parameters. The result was a ranking of these parameters in order of impact on safe operating power level.[4] The second- and fourth-ranked parameters were, respectively, fuel segregation (a measure of localized fuel overloading) and integrated hot streak (a measure of cumulative fuel overloading along a coolant streamline). These high rankings emphasized the importance of an accurate statistical description of the fuel distribution within ANS fuel plates.

1.4 PREVIOUS ESTIMATES OF FUEL LOADING STATISTICS

At the time that this sensitivity check was made, there were no data available pertaining to fuel loading within the ANS reactor's uranium silicide (U_3Si_2) fueled plates. The nearest approximation came from inspection data and manufacturing specifications for the HFIR's uranium oxide (U_3O_8) fueled plates. HFIR plates had always been inspected for fuel loading homogeneity, but this inspection had been on a pass/fail basis that did not lend itself to a complete statistical analysis.[5] Inspection records did indicate, however, that approximately 1% of all plates manufactured were rejected because of a localized spot (2 mm diam) overloaded with fuel at least 30% above the nominal amount. Also, approximately 1% of all plates manufactured were rejected because of an average of at least 10% overload over a streak 2 mm wide radially by 1.27 cm long in the axial direction. These data were used to estimate a mean and a standard deviation for fuel segregation and integrated hot streak for use with the Monte Carlo input to the TASHA code.[6]

This statistical estimation was inadequate for a number of reasons. First, the 1% rejection fraction pertained to plates manufactured with U_3O_8, not with U_3Si_2 fuel. Second, the pass/fail inspection data revealed nothing about the location of fuel defects: the simple extrapolation of the rejection fraction to a descriptor of fuel loading implied that overloading occurred at random locations within each fuel plate. These data did not provide sufficient detail: it was important to know the location of overloaded spots and streaks as well as their frequency.

1.5 THE PRESENT ANALYSIS BASED ON DETAILED DATA

In 1992 the fuel plate inspection equipment at Babcock and Wilcox was upgraded to accommodate digital data acquisition and storage.[7] The present work is based on the first data sets that were generated by subjecting the experimental plates to the improved inspection process. This report begins with a description of the plates and the homogeneity analysis equipment. Numerical treatment of the data is presented next, along with graphical images of the fuel loading data. Concerns are addressed regarding the effect of a change in fuel type on the data. The final sections of the report cover the statistical treatment of the data: defining subdivisions of the plates that can be adequately represented by known distributions and evaluating means and standard deviations for those distributions.

2. FUEL LOADING MEASUREMENT

2.1 FUEL PLATE DESCRIPTION

The fuel plates examined for this study were identical to HFIR outer element plates except that the HFIR's uranium oxide fuel was replaced with uranium silicide at slightly higher areal uranium loadings. The configuration was the same: a laminar assembly of radially contoured fuel meat and aluminum powder filler, clad between outer laminations of 6061 aluminum plate.[8] These plates differed from ANS fuel plate design in that the fuel meat did not have an axially graded contour.

All HFIR plates are inspected for hot spots (local regions of overloading), hot segments (short axial regions of overloading), and overall fuel loading as part of the manufacturing process.[9] Fuel loading is reported in units of percent deviation from nominal loading. Percent deviation (PD) may be defined as

$$PD = \frac{m_{m,l} - m_{n,l}}{m_{n,l}} \times 100\% \quad , \tag{1}$$

where

$m_{m,l}$ = local measured fuel mass,
$m_{n,l}$ = local nominal fuel mass.

HFIR criteria reject plates if a local PD is >+27% or if a 1.27-cm (0.5-in.) segment shows an average PD >±12%. The ANS uncertainty analysis required statistics for PD as a continuous variable; thus, a first step in the present work was to convert the output from HFIR's discrete stepped measurement system to a system that provided continuous information on PD.

2.2 X-RAY ATTENUATION SCANNING

Fuel loading is measured by observing the attenuation of a collimated 2-mm-diam X-ray beam as it passes through a fuel plate.[5] The data are supplied in units called "counts" that increase with higher fuel loading. More fuel in a given plate volume causes more attenuation of the beam, but the exact relationship between fuel loading and counts is not known analytically.

The X-ray beam scans along the fuel plate in a raster pattern. Data are collected at discrete intervals and averaged every seven readings. This average is reported as a counts datum. There are 521 data points, called "positions," along the axial length of the scan, each spaced 1.52-mm (0.06-in.) apart. Each axial scan is called a "track." Tracks increment in the radial direction, with a 1.52-mm (0.06-in.) spacing for outer plates. Figure 2.1 is an illustration of the scanning arrangement, showing the track and position axes. The fueled region occupies the largest area of the scan; the standards region (explained below) is on the left. The "end clad" is part of the aluminum frame that surrounds the fueled region. Figure 2.2 is a three-dimensional plot of a typical counts data set as provided by the homogeneity scanner. The standards are visible on the left, and the fueled region is the large area on the right. The high "walls" are regions of high attenuation caused by support beams beneath the fuel plate in the scanning apparatus. The radial contour characteristic of HFIR fuel loading is visible in Fig. 2.2, with more fuel (and thus higher attenuation) toward the radial center of the plate.

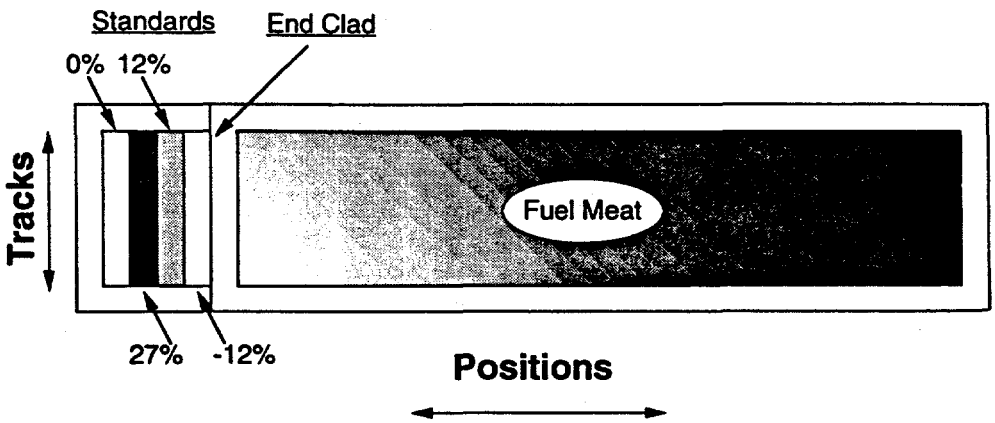

Fig. 2.1. Homogeneity scanner setup.

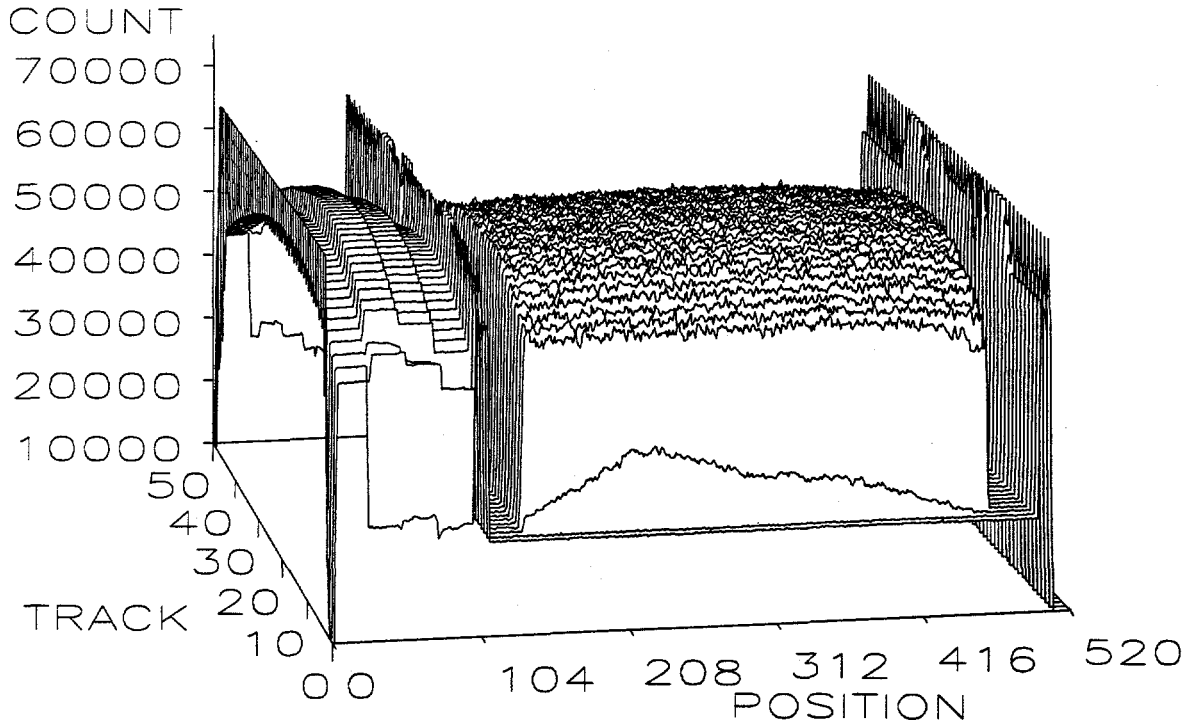

Fig. 2.2. Counts data plotted as a function of track and position.

3. REFERENCE STANDARDS

The unknown relationship between fuel loading and counts means that counts data cannot be neatly translated into a measurement of fuel mass by some analytical function. Instead, reference standards are placed in the scan path to provide a calibration between counts and PD. The standards are milled from blocks of 6061 aluminum and cut so that at any given radial location they provide X-ray attenuation (and thus counts) identical to those of a fuel plate of known loading. Destructive sampling and chemical analysis of fuel plates was used to develop the standards. Standards representing PD values of –12%, 0% (nominal), 12%, and 27% are used for each scan. Interpolation of counts fuel data between these PD values allows the raw counts data sets to be converted into continuous PD data sets. The PD data sets represent actual fuel loading in the plates.

The axial length of the standards is such that each contains about 25 position data points. The standards are milled with great precision. The combined effects of physical fluctuations in the standards and instability in the X-ray beam amount to only a 0.2% variation in the standards data. As explained below, this represents a PD error of ±0.5% in the indicated fuel loading.

3.1 STANDARDS WIDTH

The standards must extend far enough in the radial direction to cover the entire design width of the fuel meat region. For an outer plate, this includes tracks 2 through 48. While not needed for homogeneity analysis, standards data for tracks 0, 1, 49, and 50 can be used to check for the presence of fuel outside of design boundaries. Close examination of scan data reveals that the edges of the standards do not always provide usable data. Along these edge tracks a standard may produce counts data that are unusually low, have an unusually high variance, or both (see Fig. 3.1). The error thus caused in the PD calculations for the edge tracks is unacceptably large.

3.2 EXTRAPOLATING STANDARDS DATA

A remedy for the bad data at the edges of the standards is to throw them out, replacing them with values extrapolated from good data on the standards. Fortunately, the standard representing 0 PD for the outer plate design provided good data over the standard's full width, from tracks 0 to 50. The counts values generated by the 0 PD standard on tracks 0 through 2 and tracks 46 through 50 were thus used as a base from which to extrapolate counts values for the other standards along the same tracks. The good data for the –12, +12, and +27 PD standards extended outward to track 3 on the low end and to track 45 on the high end. The ratio of counts values between the standards at these outermost good tracks was assumed to be constant out to the edges of the standards. An example demonstrates the extrapolation of a counts value for the 27 PD standard along track 0:

$$\text{27 PD standard for track 0} = \text{0 PD standard for track 0} \times \frac{\text{27 PD standard for track 3}}{\text{0 PD standard for track 3}} , \quad (2)$$

where all values are counts (actually, the mean of the 25 counts values generated by that standard along that track). Similar extrapolations were made for tracks 1 and 2 and for the –12 and +12 PD standards. This process was repeated for the other edge of the standards, using data from track 45 to

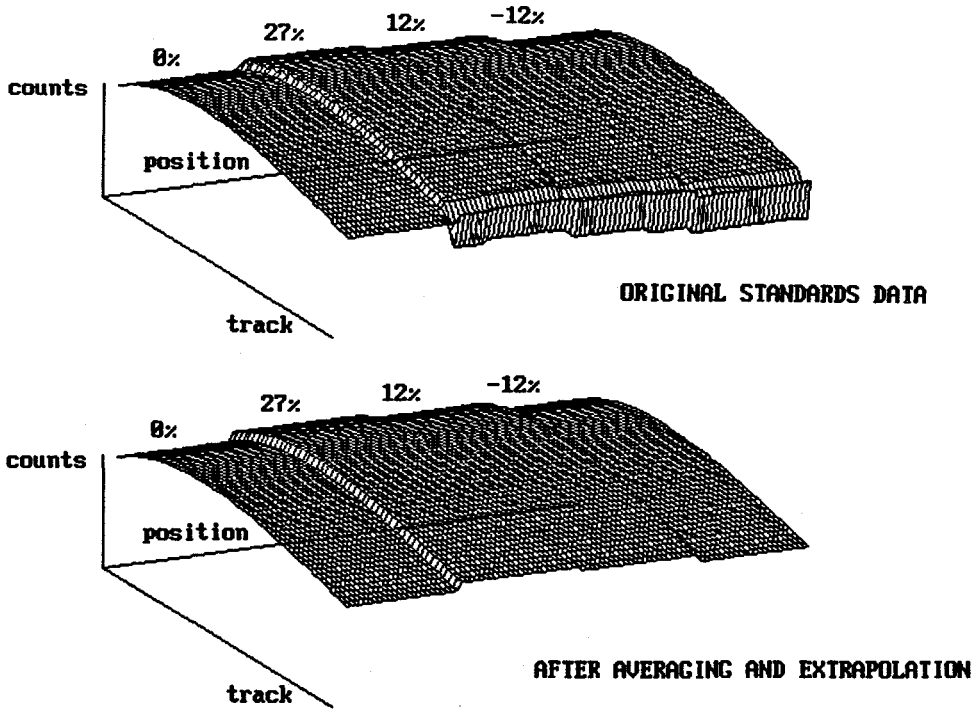

Fig. 3.1. Closeup of counts data in standards region.

form the ratio. Figure 3.1 shows a three-dimensional plot of the standards data before and after the extrapolation was performed.

4. CONVERSION OF COUNTS TO PERCENT DEVIATION

The corrected standards data were used to convert counts values to PD values for every data point in the scan data set. A curve was fitted for each track, relating PD to counts in a piecewise-linear function. Five points of the form (PD, counts) were tabulated for each track, and a straight line was generated between each of the points. Four PD values were taken from the standards (i.e., –12, 0, 12, and 27%). The counts values were the means of the 25 or so data points in the scan data set that corresponded to a particular standard along a particular track.

The fifth point was generated by assuming that the end clad region of the fuel plate represented a –100% standard. The mean of the counts data in the aluminum end clad along that track was paired with the –100% value to form the fifth point. This step was partially justified by the definition of PD: –100% means zero fuel mass, and there was no fuel mass in the end clad. This method, however, neglected the effect of the aluminum on X-ray attenuation. In thinner fuel meat regions, the aluminum was thicker, and the aluminum had some effect on the counts values. This effect has not been quantified, and for the time being, the effects of the aluminum were neglected. After all, that the main purpose of this analysis was to look for overloading in the fuel plates. The –100 PD data point affected only underloaded regions with PD values between –100 and –12 PD.

The bulk of the uncertainty in the resulting PD values resulted from the variance in the counts data. The uncertainty was assumed to be one standard deviation of the counts values multiplied by the slope of the line in the appropriate segment of the piecewise-linear function. There was a slightly different uncertainty associated with each data point in each piecewise-linear curve. In the PD data set, then, on a given track, there was some uncertainty for values near 0 PD, a slightly different uncertainty for values near 12 PD, and so on. In general, these uncertainties were $<\pm 0.5$ PD. There was some error added by the extrapolation of the standards data to the edge tracks, but the extrapolation was only over one or two tracks. This error was not quantified, but Fig. 3.1 allows a visual check on the results of the extrapolation.

Each track, then, had its own continuous, piecewise-linear function relating PD to counts. Counts values were converted to PD values by using the counts values as the argument for the function at each data point along the track. Figure 4.1 presents the results of this conversion. Fourteen data sets are shown as maps of PD plotted by track and position. The oxide-loaded plate is data set o195901; all of the other images are of silicide-fueled plates. Data set 1320201 is included only to demonstrate the response system to overloading above 27%; this data set was excluded from all statistical analyses. The HFIR standards values of –12, 0, 12, and 27% were used as breakpoints between the regions when creating the images.

Figure 4.1 reveals a number of features of the PD data sets. Figure 4.2 serves as a guide. The standards regions (1) are plainly visible. They have a mottled appearance because of small variations above and below nominal PD within each standard. The fueled region (2) is visible, surrounded by the frame (3). The narrow bars (4) are regions of high attenuation caused by steel supports that held up the plates during the homogeneity scan. All of the data sets show a subtle but consistent skew in fuel loading: PD values are lower near the radial edges and higher near the middle. It is obvious that different regions of the plates have different loading characteristics; these differences were quantified during the statistical analysis. Also note that all of the silicide plates in Fig. 4.1 appear to be underloaded. In fact, this is a measurement error caused by using oxide fuel reference standards with silicide fuel. Similar measurement errors resulting from changes in fuel types were encountered and corrected in the 1970s by Texas Instruments, Inc.[10] These cases involved oxide fuel with a higher than nominal fraction of fine particles and a fuel containing "burned oxide" particles. The next section explains the correction made to the PD data sets to offset this error for silicide fuel.

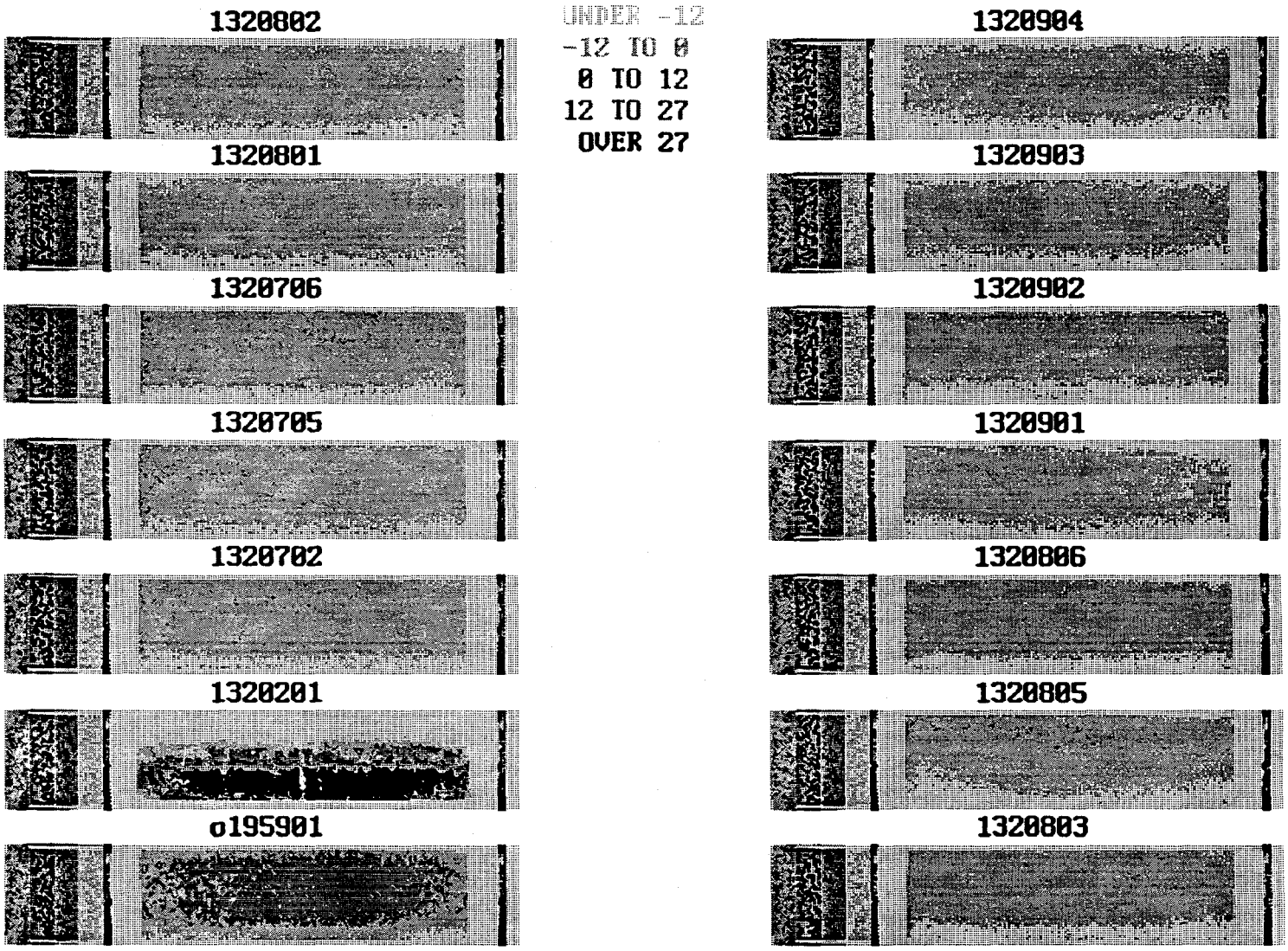

Fig. 4.1. Uncorrected oxide and silicide homogeneity scans (PD).

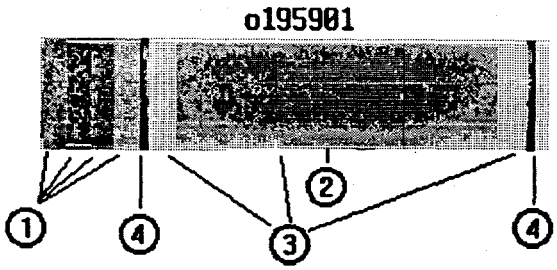

Fig. 4.2. Guide to image features.

Finally, note the numbering system used for the homogeneity scan data sets. The oxide fuel scan begins with the letter *o*. The silicide fuel scans begin with the numbers *132*, concatenated with the number of the fuel lot used to make the plate. Thus plates 1320702, 1320705, and 1320706 all contain fuel from lot 700.

5. OVERALL PERCENT DEVIATION

The PD values were used to calculate a quantity called the overall percent deviation (OPD) for each fuel plate. OPD was intended to be a measure of the fuel loading in the plate as a whole, but was also used to correct the PD data sets for the error that caused the silicide plates to appear underloaded. OPD integrated local PD values across the fueled region of a fuel plate, while adjusting for local variations in fuel thickness. A definition of OPD is

$$OPD = \frac{m_{m,t} - m_{n,t}}{m_{n,t}} \times 100\% \quad , \tag{3}$$

where

$m_{m,t}$ = total measured fuel mass,
$m_{n,t}$ = total nominal fuel mass.

The total measured fuel mass is calculated as:

$$m_{m,t} = A_l th_{max} U_{loading} \times \sum \left[\left(\frac{PD}{100\%} + 1 \right) th_{rel} \right] \quad , \tag{4}$$

where

A_l = local area represented by each 0.0236-cm^2 data point,
th_{max} = maximum thickness, the fuel meat thickness at a relative thickness of unity (0.0106 cm according to fuel plate design specifications; this occurs near track 17 in the outer plate design),
$U_{loading}$ = uranium loading (from manufacturing data, see Appendix B),
th_{rel} = relative thickness, describing the fuel contour at a given point (from fuel plate design specifications, see Appendix A).

$U_{loading}$ is reported in units equivalent to density, i.e., mass per unit volume. Note that the terms within the summation are values that change with location, i.e., with each data point. The terms outside of the summation are constant over the entire fueled region. Combining Eqs. (3) and (4), then,

$$OPD = \frac{A_l th_{max} U_{loading} \times \sum \left[\left(\frac{PD}{100\%} + 1 \right) th_{rel} \right] - m_{n,t}}{m_{n,t}} \times 100\% \quad . \tag{5}$$

Equation (3) shows OPD to be the difference between measured fuel mass and nominal fuel mass, expressed as a percentage. Accountability during fuel plate manufacture meant that the mass of fuel that went into the plate was known rather precisely. OPD readings were thus expected to be very close to zero. It must be emphasized that PDs and thus OPDs were generated by comparison against reference standards that represented plates loaded with oxide fuel. Reference standards for silicide-loaded plates were not available for this analysis; thus plates loaded with uranium silicide fuel were

compared against oxide reference standards. The remainder of this section discusses this problem and demonstrates how the OPD was used to recalibrate the standards for use with silicide fuel.

5.1 IMPACT OF SILICIDE FUEL ON HOMOGENEITY SCAN DATA

The difference in fuel types caused a downward shift in counts readings, PDs, and OPDs for silicide-loaded plates. Two major contributors to this shift were believed to be higher fuel density and a different particle size distribution for the silicide fuel (the particle size distribution for the silicide fuel was more heavily weighted toward larger particles). Thus fewer particles were necessary to load the plate with the same mass of uranium, and those particles were likely to be larger than oxide particles. This difference was believed to decrease the probability that a beam of X-rays would be attenuated by striking a fuel particle. The X-ray scanning apparatus reported these fewer, larger particles as lower counts. Unfortunately there was no mathematical model available to predict these effects explicitly. Thus it was not possible to calculate fuel loading from counts data for silicide fuel by means of some physically derived function. To gain an appreciation of the problem's magnitude, examine Table 5.1.

Table 5.1. Effect of fuel mass and uranium loading on overall percent deviation

Plate	OPD with oxide specs (%, ±0.5)	OPD with silicide lot specs (%, ±0.5)
o195901	0.0	
1320702	–7.5	–3.0
1320705	–7.5	–3.0
1320706	–7.5	–3.0
1320801	–8.5	0.0
1320802	–8.5	0.0
1320803	–8.5	0.0
1320805	–8.5	0.0
1320806	–8.5	0.0
1320901	–10.0	–2.0
1320902	–10.5	–2.0
1320903	–10.5	–2.0
1320904	–10.5	–2.5

The table shows for each plate the OPD as calculated with mass and density data from oxide fuel and the OPD calculated with mass and density data from silicide fuel lots (these data appear in Appendix B). The reference standards assumed the total fuel mass and uranium loading specifications for oxide-fueled plates; thus they caused low readings when applied to silicide-fueled plates. When OPDs were corrected for known differences (i.e., calculated with total fuel mass and uranium loading data from silicide fuel lots), the shift was fully compensated for one fuel lot (800), but not for lot 700

or lot 900. This failure to account fully for shifts in OPD may have resulted from particle size parameters.

5.2 CONVERTING OXIDE REFERENCED SCAN DATA FOR SILICIDE FUEL USING OVERALL PERCENT DEVIATION

The previous section showed that correcting for fuel mass and density improved the calculated OPD for silicide-fuel plates. In the absence of a more complete understanding of the problem, it was decided to force numerically the (oxide spec) OPD for each silicide plate data set to zero. A function was derived to adjust the PD data, thus achieving an OPD of zero.

Equation (3) has shown the OPD to be the difference between total measured fuel mass and total nominal fuel mass in the plate, expressed as a percentage. Two assumptions allow the OPD to be defined locally, as well as over the whole plate. This is a first step toward correcting locally measured fuel masses for the error caused by differences in fuel types. The assumptions may be stated as follows:

1. The plate contains the total reported fuel mass; i.e., there is no fuel missing. The OPD is therefore an artifact of the measurement technique.
2. The OPD is constant over all locations in the fuel plate.

Assumption 1 justifies an attempt to force the OPD numerically to a value of zero, thus negating the effects of the measurement error. Assumption 2 implies that the OPD, once calculated over the total plate by Eq. (5), can be applied locally to correct the error in local fuel mass measurements (these assumptions were used implicitly, but not explicitly stated in Ref. 10). Appendix C contains a more complete analysis of these assumptions. Given assumptions 1 and 2, OPD is redefined on a local basis:

$$OPD = \frac{m_{m,l} - m_{c,l}}{m_{c,l}} \times 100\% \quad , \tag{6}$$

where

$m_{m,l}$ = local measured fuel mass,
$m_{c,l}$ = local corrected fuel mass.

Contrast the use of $m_{c,l}$ in Eq. (6) with that of $m_{n,l}$ in Eq. (1) In Eq. (1), $m_{n,l}$ is known and represents the local mass of fuel that would exist if there were no deviation from nominal fuel loading. In Eq. (6), $m_{c,l}$ is unknown and represents the mass of fuel that would be measured if there were no error caused by differences in fuel types. By solving Eq. (6) for $m_{c,l}$, the OPD can be used to correct local mass measurements.

$$m_{c,l} = \frac{m_{m,l}}{\left(\frac{OPD}{100\%} + 1\right)} \quad . \tag{7}$$

Fuel loading is measured as PD, however, not mass; so, the corrected percent deviation (CPD) is defined similarly to PD in Eq. (1).

$$CPD = \frac{m_{c,l} - m_{n,l}}{m_{n,l}} \times 100\% \quad . \tag{8}$$

CPD is PD as corrected for differences in fuel types. To develop a function to convert PD to CPD, first rearrange Eq. (1)

$$m_{m,l} = m_{n,l}\left(\frac{PD}{100\%} + 1\right) \quad . \tag{9}$$

Combine Eqs. (7) and (8)

$$CPD = \frac{\left[\frac{m_{m,l}}{\left(\frac{OPD}{100\%} + 1\right)}\right] - m_{n,l}}{m_{n,l}} \times 100\% \quad , \tag{10}$$

and incorporate Eq. (9)

$$CPD = \frac{\left[\frac{m_{m,l}\left(\frac{PD}{100\%} + 1\right)}{\left(\frac{OPD}{100\%} + 1\right)}\right] - m_{n,l}}{m_{n,l}} \times 100\% \quad . \tag{11}$$

Then simplify:

$$CPD = \frac{PD - OPD}{\left(\frac{OPD}{100\%} + 1\right)} \quad . \tag{12}$$

Equation (12) is the function used to convert PD to CPD, correcting the error in measured fuel mass (and thus in PD) by means of the OPD. Figure 5.1 is a plot similar to Fig. 4.1, but with the PD values replaced by CPD values. Notice the similarity between the silicide plates and the oxide plate after the correction. In both cases, only a few local points in the fuel are seen to exceed 12 PD, and these occur near the middle of the plate. Also note that the standards data have been "corrected" as well as the

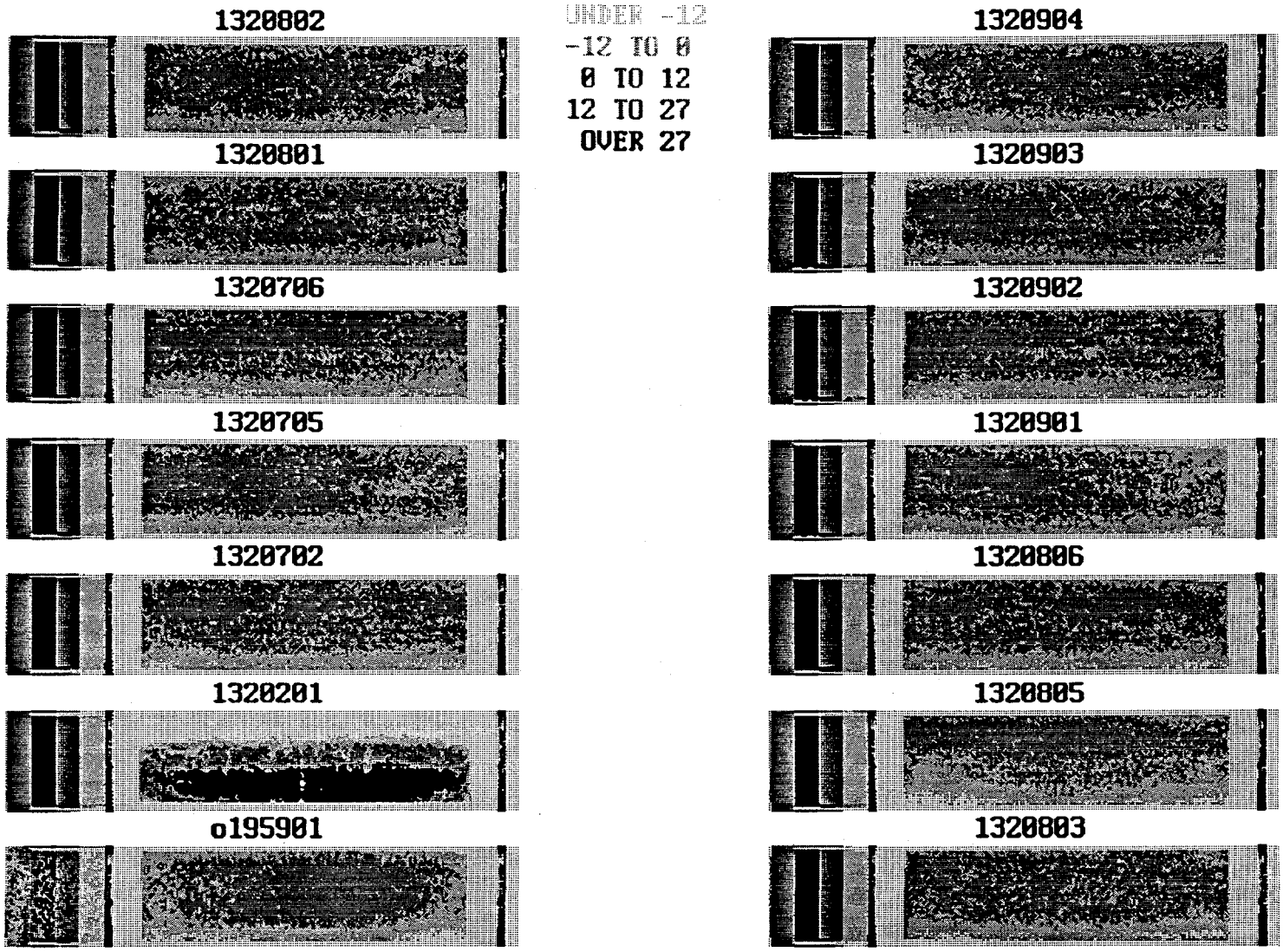

Fig. 5.1. Corrected oxide and silicide homogeneity scans (CPD).

fuel data in the silicide scan; thus the standards now read too high. This fact is of no consequence, however, because the standards were used only to generate PD values from the original counts data, not to correct from PD to CPD. The oxide plate's data set was also converted from PD to CPD so that a direct comparison between this data set and the silicide plates' data sets would remain valid. The OPD for the oxide fuel plate was very close to zero; thus CPD and PD values (and the resulting scan images in Figs. 4.1. and 5.1) for the oxide plate are almost identical.

6. STATISTICAL ANALYSIS OF FUEL PLATES

6.1 ISOLATING THE FUELED REGION

Twelve silicide-loaded plates (lots 700, 800, and 900) were analyzed. The fueled region of a typical plate can be seen by creating a three-dimensional plot of the corresponding counts data set, as in Fig. 6.1.

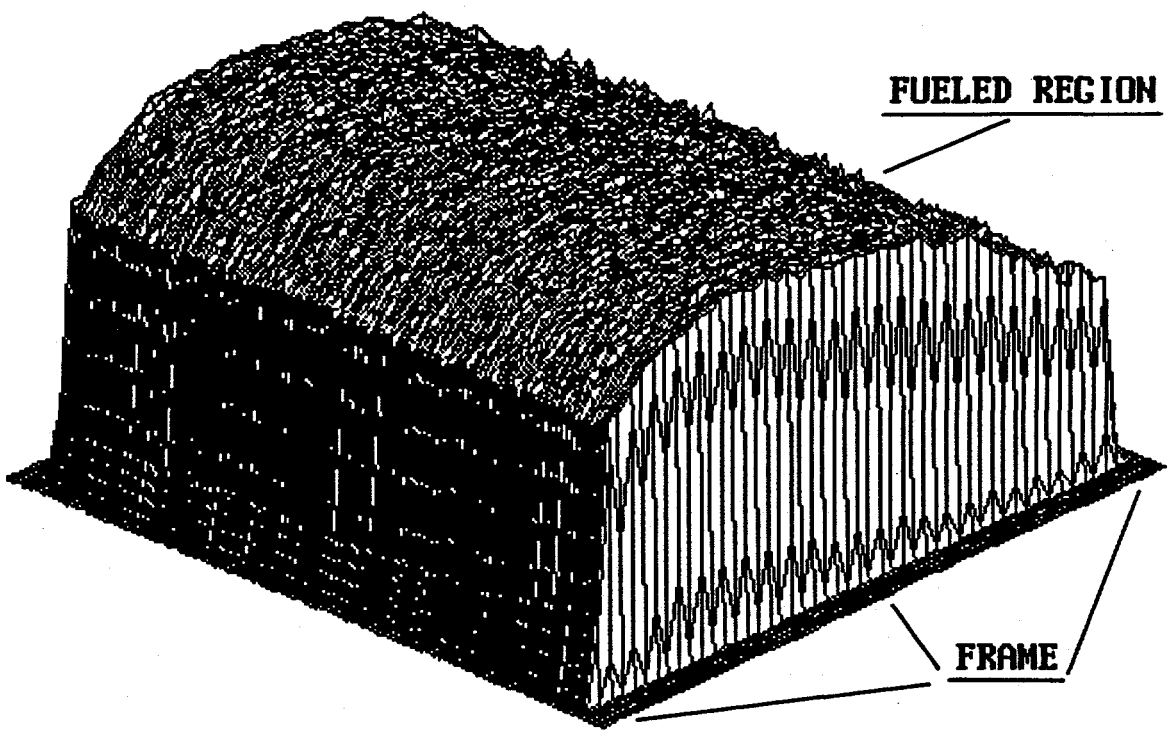

Fig. 6.1. Scan data for fueled region.

The fueled region appears to rise in relief from the aluminum frame surrounding it. Close examination allows maximum and minimum values to be assigned to tracks and positions for the fueled region of each data set.

Fueled regions do not have perfectly abrupt and straight edges, and the collimated beam may strike a combination of frame and fuel meat. Thus one or two tracks or positions surrounding a fueled region will show slight fuel loadings. The fuel loading values in these margins are very low, with CPD values from –15 to –100%. Including these low values in statistical subsets tends to reduce mean values and to increase the variance for those subsets. To avoid such problems, only the bulk of the fueled regions is considered in the statistical analysis described below. In the radial direction, bulk fueled regions run from tracks 3 to 47 for all data sets. Axially, the bulk fueled regions vary slightly in length and

position, extending between approximately positions 146 to 471. These tracks and positions represent an area 6.7 cm by approximately 49.5 cm.

6.2 LOCAL ANALYSIS

The resolution with which PD could be measured was limited by the X-ray beam spot size in the homogeneity scanning apparatus. It was desired to represent statistically the fuel loading variations at as fine a resolution as possible; hence data sets made up of local CPD values were collected. The fueled portion of the plates was divided into axial and radial regions for this analysis. The divisions were made to accommodate separate statistical descriptions of various portions of the plates. Each region would be described by the mean and standard deviation of the local values within each region. For such a description to have meaning, however, it was important that the set of local values in each region represent a sample from a population with a known distribution. Histograms formed from the data tended toward normal, as opposed to other distributions; thus regions were sought that showed normal distributions of local values.

In the axial direction, the length of the fueled portion of the plates was divided into fourths. These axial divisions were labeled 0 to 25% length, 25 to 50% length, etc. In the radial direction, there were 45 tracks on each plate that contained a significant amount of fuel. Various groupings of these tracks were tested for adherence to a normal distribution (by means of the χ^2 test, described below). A compromise was sought to minimize the number of radial divisions, while maintaining a reasonable adherence to normal distributions within the regions so defined. Once the divisions between the axial and radial regions were established, data sets were drawn up of local values within these regions for all 12 fuel plates combined and were tested for mean, standard deviation, and the χ^2 statistic.

6.3 χ^2 TEST FOR NORMAL DISTRIBUTIONS

One way to check for normal distributions was to look for the familiar "bell" shape in histograms formed from the data sets. It was desirable, however, to supplement this subjective approach with an objective test for adherence to normal distributions. This was found in the χ^2 test.[11] The χ^2 test was used to test for goodness of fit between an observed frequency distribution and a theoretical distribution. The χ^2 statistic is defined as

$$\chi^2 = \sum_{i=1}^{k} \frac{(o_i - e_i)^2}{e_i} \quad , \tag{13}$$

where

k = the number of terms used in the summation (i.e., the number of bins in the histogram),
o_i = observed frequencies,
e_i = expected frequencies.

The sampling distribution of the χ^2 statistic is approximated by the χ^2 distribution with k–m degrees of freedom, where m is the number of values required to generate the expected frequencies (in this case, m = 3: mean, standard deviation, and number of data points).

This test was used to compare the frequency distribution of local CPDs with the frequencies occurring in a normally distributed population having the same mean and standard deviation as the sample set. The null and alternative hypotheses were stated as:

H_0: The frequency distribution represents a random variable with the normal distribution having a mean, μ, and a standard deviation, σ.

H_a: The frequency distribution represents a random variable that does not have this normal distribution.

The level of significance was chosen at 0.01. Thus the probability of a type I error, i.e., a false rejection of the null hypothesis, was 0.01. The null hypothesis was rejected if the calculated χ^2 value exceeded the tabulated value for $\chi^2_{(0.01)}$ with three degrees of freedom.

6.3.1 Observed Frequencies

Observed frequencies were calculated from the data set by grouping the data into bins of equal width. The mean, μ, and standard deviation, σ, of the data set were used to size and locate the bins. The centers of the lowest and highest bins were placed at

$$\text{low bin} = \mu - 3\sigma \tag{14}$$

and

$$\text{high bin} = \mu + 3\sigma \quad , \tag{15}$$

respectively. The bin width, w, was calculated as

$$w = \frac{\text{high bin} - \text{low bin}}{20} \quad , \tag{16}$$

thus creating 21 bins. The data were grouped into these bins to create the observed frequency distribution.

6.3.2 Normal Probabilities and Expected Frequencies

A normal probability curve was generated using the following function:

$$Norm = f(x;\mu,\sigma) = \frac{1}{\sqrt{2\pi}\,\sigma}\exp\left[-\frac{(x-\mu)}{2\sigma^2}\right] \quad , \tag{17}$$

where x is the value of the random variable, in this case, CPD.

To perform the χ^2 test, the normal probability curve was scaled up by a factor of (wn). This step converted the normal probability curve into a plot of expected frequency values for a sample of a random variable of sample size n, mean μ, and standard deviation σ. Observe that the scaling factor (wn) is actually the area under the observed frequency histogram and is equal to the area under the expected frequency curve.

In general, each term in the χ^2 summation of Eq. (13) was evaluated at the center of each bin in the histogram. Note, however, that the observed and expected frequencies were clustered together so that none of the expected frequencies was less than five.[12] The number of terms in the χ^2 summation, k, was thus variable and was smaller for smaller data sets. The χ^2 test was performed for each data set by testing whether χ^2 exceeded $\chi^2_{(0.01)}$.

6.3.3 Interpreting χ^2 Test Results

As mentioned above, the χ^2 test was used to compare the frequency distribution of local fuel loadings with the frequencies occurring in a normally distributed population having the same mean and standard deviation as the sample set. A rejection of the null hypothesis, however, did not render a data set useless. None of the data sets sampled from local CPD values, in fact, "passed" the χ^2 test.* Rather, the calculated χ^2 values were used as a scale with which to judge the goodness of fit of the sample set with a perfectly random, normally distributed population. There was no reason to think that a different kind of distribution other than normal would have provided a better fit to the data. Comparison of numerical χ^2 results with graphical histograms of the respective confirmed this belief.

6.4 LOCAL ANALYSIS RESULTS

Table 6.1 presents the results of the local analysis in a numerical format, while Fig. 6.2 presents these results as histograms. The histograms in Fig. 6.2 are overlaid with curves representing a normal distribution.

Comparison of the χ^2 results in Table 6.1 with the histograms in Fig. 6.2 points up the danger in adhering too closely to acceptance or rejection of the assumption of normality based strictly on the χ^2 test result. The histograms make it plain that the data sets can be adequately represented by a random sampling from a normally distributed population having the same mean and standard deviation as the data set. The χ^2 test results are most useful as an indicator of variation in the distributions between different regions of the fuel plates. Generally, distributions tend more toward normal in the center of the plates and are less normal toward the edges and corners.

6.5 HOT SEGMENT ANALYSIS

One of the criteria for accepting HFIR fuel plates has been a limit of ±12 PD in fuel loading averaged over a 1.27-cm (0.5-in.) axial length along any given track. This measurement was adopted in the present analysis as another statistical description of fuel loading for the homogeneity scan data sets. CPD data sets were rewritten by averaging eight consecutive CPD values along each track and

---

*The nature of the χ^2 test is such that larger data sets will be less likely to "pass" the test. To an extent, this probability is intuitive: as more data are sampled from a truly normally distributed population, the frequency distribution should, indeed, approach the standard normal distribution. It seems, however, that the χ^2 test gets too rigorous for large data sets. With reference to Eq. (13), note that the magnitudes of the values in the numerator inside the summation will increase with larger data sets. The absolute value of the numerator will thus also increase; this increase is then squared. The result is that frequency distributions from large data sets may produce histograms that visually appear quite normal, but are soundly rejected by the χ^2 test. This conflict between judgment and statistical test results has not been resolved and warrants further inquiry.

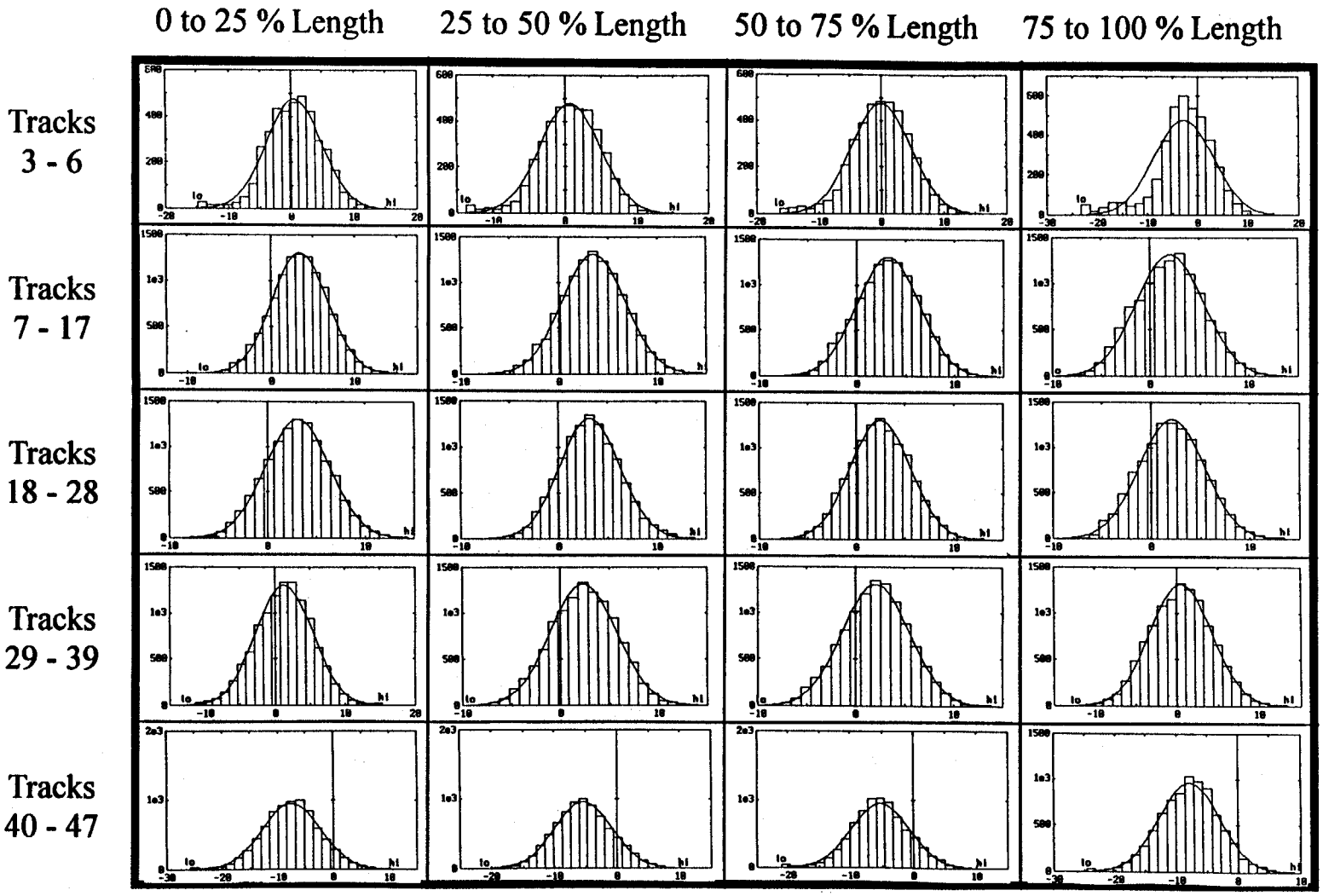

Fig. 6.2. Local CPD distributions.

Table 6.1. Local analysis results

Tracks	Means and standard deviations							
	0 to 25% length		25 to 50% length		50 to 75% length		75 to 100% length	
	μ	σ	μ	σ	μ	σ	μ	σ
3–6	0.43	4.41	0.63	4.19	–0.05	4.73	–2.77	5.92
7–17	3.48	3.33	3.53	3.20	3.21	3.17	2.00	3.40
18–28	3.09	3.27	3.19	3.08	2.47	3.06	2.08	3.29
29–39	1.32	4.05	2.33	3.37	2.06	3.41	0.50	3.73
40–47	–7.57	5.26	–5.40	4.53	–5.28	4.57	–7.91	4.88
	χ^2 Test results							
	χ^2	$\chi^2_{(0.01)}$	χ^2	$\chi^2_{(0.01)}$	χ^2	$\chi^2_{(0.01)}$	χ^2	$\chi^2_{(0.01)}$
3–6	282	35	347	35	325	35	1004	35
7–17	50	38	67	38	80	38	109	38
18–28	64	38	81	38	86	38	119	38
29–39	140	38	63	38	63	38	44	38
40–47	115	35	37	35	209	35	130	35

then replacing the first data point of the eight with the average value. One CPD data point at a time was thus converted to a hot segment data point until there were fewer than eight data points remaining for a given track. Data sets were truncated at that point so that hot segment data sets ended up eight data points shorter than CPD data sets in the axial or "position" direction. The statistical analysis with the plate divided into regions for mean, standard deviation, and χ^2 tests was performed just as it was for the local analysis.

6.6 HOT SEGMENT ANALYSIS RESULTS

Table 6.2 presents the results of the hot segment analysis in a numerical format, while Fig. 6.3 presents these results as histograms. The histograms in Fig. 6.3 are overlaid with curves representing a normal distribution.

The results of the χ^2 test for the hot segment regions are similar to those for the local analysis. Only one region "passes" the test, but the histograms again indicate that the assumption of normal distributions is reasonable. Note that the averaging of local values into hot segment values resulted in means that are quite similar, but significantly affected the variance of the regions' data sets. Standard deviations are consistently lower for the hot segment regions because of this averaging.

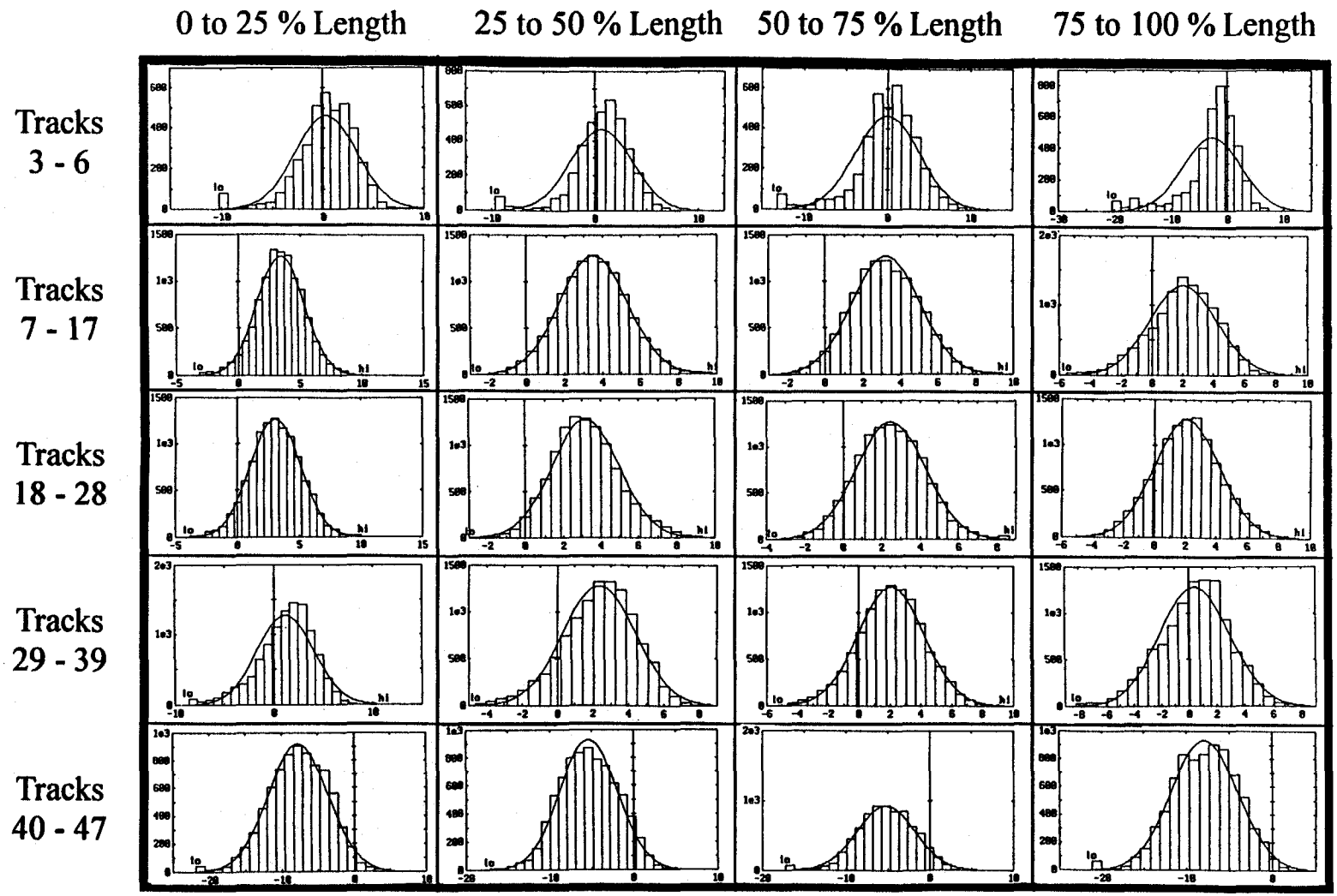

Fig. 6.3. Hot segment CPD distributions.

Table 6.2. Hot segment analysis results

Tracks	Means and standard deviations							
	0 to 25% length		25 to 50% length		50 to 75% length		75 to 100% length	
	μ	σ	μ	σ	μ	σ	μ	σ
3–6	0.29	3.05	0.63	2.97	–0.05	3.79	–2.73	5.12
7–17	3.42	1.91	3.51	1.80	3.22	1.80	2.01	2.18
18–28	3.08	2.01	3.18	1.78	2.47	1.79	2.08	2.09
29–39	1.15	2.84	2.35	2.03	2.07	2.12	0.42	2.50
40–47	–7.73	4.11	–5.37	3.41	–5.28	3.45	–7.93	3.84
	χ^2 Test results							
	χ^2	$\chi^2_{(0.01)}$	χ^2	$\chi^2_{(0.01)}$	χ^2	$\chi^2_{(0.01)}$	χ^2	$\chi^2_{(0.01)}$
3–6	1101	35	1840	35	1514	35	2555	35
7–17	261	38	27	38	69	38	407	38
18–28	87	38	214	38	244	38	44	38
29–39	1871	38	409	38	98	38	411	38
40–47	238	35	135	35	470	35	339	35

6.7 HOT STREAK ANALYSIS

Positive PDS represent local volumes that are overloaded with fuel. These are especially important in that sustained overloading along a coolant flow channel will decrease margins to heat flux limits (e.g., critical heat flux). In an attempt to model this cumulative effect of overloading, local PD values were averaged along axial lengths of the plate in the direction of coolant flow. Along each axial track, values were averaged to 25, 50, 75, and 100% of the plate length. For hot streak analysis, then, the approximately 300 local PD values along each track were replaced by four mean values for that track. Note that these were cumulative average, i.e., 0 to 25%, 0 to 50%, 0 to 75%, and 0 to 100% length. The statistical analysis used regions identical to those used for the local and hot segment analyses described above, but with much smaller statistical data sets because of the cumulative averaging. As an example, the 25%-length region 1 data set contained four mean values from each plate (one mean value each for tracks 3, 4, 5, and 6). Twelve plates' data sets were combined; thus 48 values were analyzed for mean, standard deviation, and χ^2 comparison with normal distribution.

6.8 HOT STREAK ANALYSIS RESULTS

Table 6.3 presents the results of the hot streak analysis in a numerical format, while Fig. 6.4 presents these results as histograms. The histograms in Fig. 6.4 are overlaid with curves representing a normal distribution.

Table 6.3. Hot streak analysis results

Tracks	Means and standard deviations							
	0 to 25% length		0 to 50% length		0 to 75% length		0 to 100% length	
	μ	σ	μ	σ	μ	σ	μ	σ
3–6	0.42	2.59	0.53	2.46	0.33	2.65	–0.45	2.96
7–17	3.36	1.23	3.35	1.05	3.28	0.93	2.92	0.94
18–28	3.15	1.52	3.22	1.25	3.03	1.01	2.80	0.98
29–39	0.92	2.19	1.57	1.68	1.71	1.47	1.32	1.46
40–47	–6.95	3.87	–5.90	3.45	–5.52	3.34	–5.98	3.33
	χ^2 Test Results							
	χ^2	$\chi^2_{(0.01)}$	χ^2	$\chi^2_{(0.01)}$	χ^2	$\chi^2_{(0.01)}$	χ^2	$\chi^2_{(0.01)}$
3–6	10	13	9	13	7	13	13	13
7–17	5	20	13	20	6	20	4	20
18–28	18	23	5	23	16	23	12	23
29–39	12	17	11	17	13	17	11	17
40–47	7	20	5	20	11	20	10	20

The results of the χ^2 test for the hot streak regions were quite different from those for the other two analyses. The hot streak analysis demonstrates that smaller data sets can more easily pass the χ^2 test. The histograms look much worse in terms of adherence to normal distribution, but the χ^2 criterion was met for all regions.

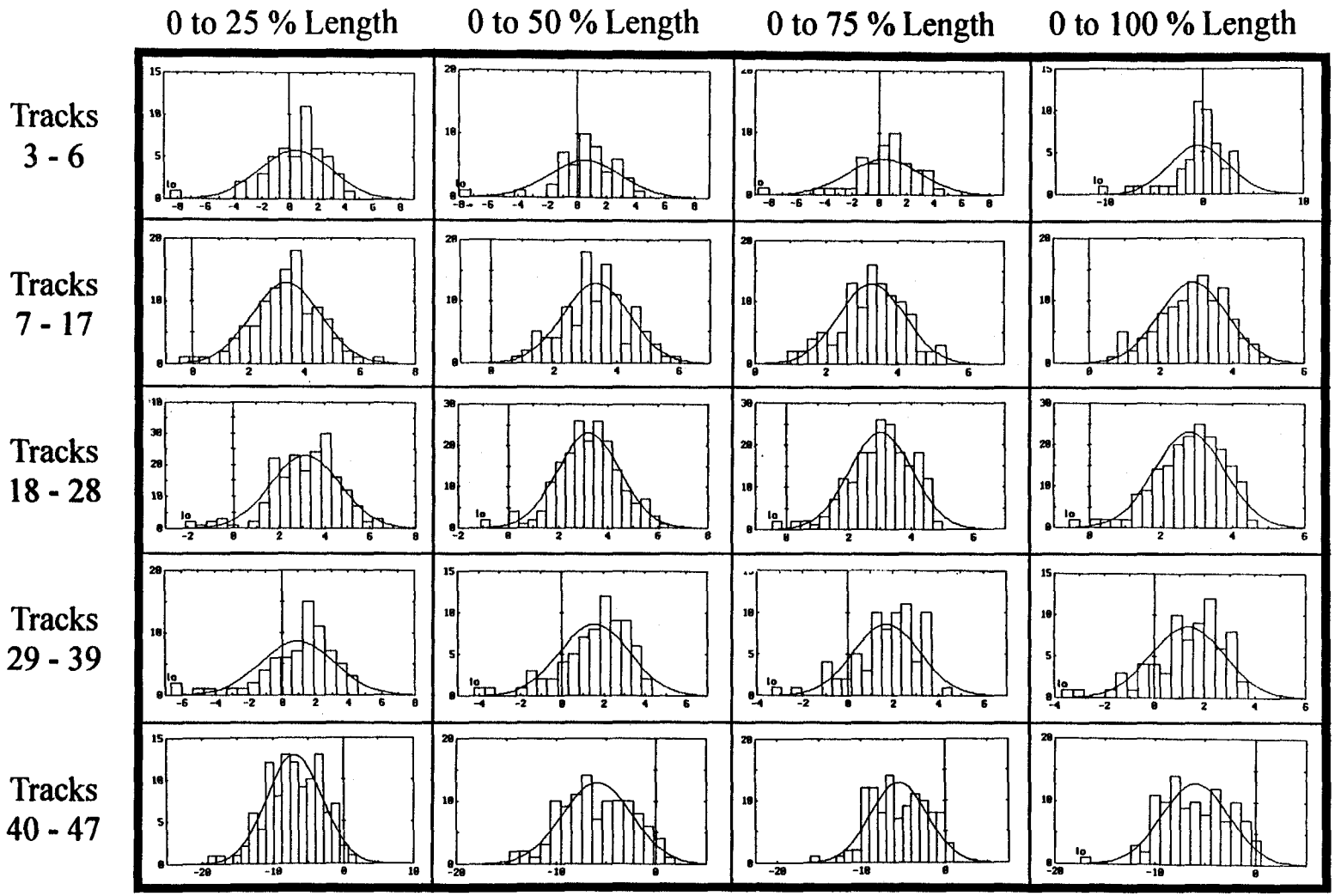

Fig. 6.4. Hot streak CPD distributions.

7. CONCLUSIONS

Data from four reference standards calibrated for HFIR fuel plates loaded with uranium oxide fuel proved sufficient to allow a statistical analysis of fuel loading and fuel loading homogeneity in experimental uranium silicide–loaded plates. The silicide fuel had an effect on X-ray attenuation that was not fully understood but that artificially lowered reported PD values from nominal fuel loading. A numerical correction to the results was made, based on assumptions of correct total fuel mass within each plate and uniformity of the PD error with respect to fuel meat thickness. Images formed from the corrected data showed loading patterns similar to loading in a HFIR plate; this process provided a qualitative check on the results.

These images and statistical analyses pointed to skewed fuel loading in the 12 silicide-loaded fuel plates studied. Fuel loading was seen to be concentrated toward the middle of the plates and attenuated near the edges. When the plates were divided into axial and radial regions, the variations in fuel loading were shown to be normally distributed. Fuel loading in these regions may thus be modeled by random samplings from normally distributed populations having the means and standard deviations reported.

It is worthwhile to note that plates from the same fuel lots as those analyzed here were subjected to destructive evaluation and dimensional analysis of fuel meat thickness. Good agreement between CPD from nominal fuel loading and PD from nominal meat thickness was observed at the thinnest portion of the fuel meat (tracks 40 to 47). At the thickest portion, CPD values indicated slight overloading, while thickness measurements indicated slightly thinner than nominal meat thickness. This disparity between the two measurements in the thick portions could be explained by a systematic fuel density variation, but it seems best to leave the question open pending accurate chemical assays of silicide-loaded plates.

8. SUGGESTIONS FOR FUTURE WORK

This analysis was based on data from only one HFIR production plate and twelve experimental plates, but each ANS reactor fuel element will incorporate hundreds of individual fuel plates. Thus, the procedures developed in this analysis should be applied to a larger base of homogeneity scan data when such data become available. For example, the OPD for the silicide plates was established here relative to a baseline of zero OPD that was observed in the single oxide plate studied. It would be preferable to establish this baseline on an average OPD value from a large number of oxide-loaded plates. It is also likely that any systematic skew in silicide plate fuel loading will corrected as part of the ANS fuel plate development process. As this development proceeds, it will be important to update the statistics presented here. It will probably be easier to improve fuel loading distributions (mean values) than it will to improve fuel loading homogeneity (variability).

Standards development is another aspect of ANS fuels development. Destructive sampling of silicide-loaded plates will provide data for homogeneity scanner attenuation as a function of uranium loading in silicide plates. These data can be used to check the validity of the hypothesis discussed in Appendix C. These data will also be applicable to development of a "standardless" system: one that employs a few known reference points and interpolates between them (such an interpolation with the HFIR standards was quite successful in the present study). Such a system would not do away with standards altogether, but there would be no need to align the standards in the scan path as is currently done.

The χ^2 test for adherence to normal distribution produced some puzzling results. It is recommended that this statistical test be studied further in this application and replaced with a more useful measure if possible.

Scan images and statistical information about fuel loading would be useful for quality assurance in fuel plate manufacture. The methodology and the computer code that were developed for the present analysis may prove useful should the need for such quality assurance arise.

9. REFERENCES

1. For more background information on ANS, see R. S. Booth, *Plant Design Requirements*, Rev. 5, ORNL/TM-11625/R5, Martin Marietta Energy Systems, Inc., Oak Ridge Natl. Lab., December 1994.

2. G. L. Yoder et al., *Steady-State Thermal-Hydraulic Analysis of the Advanced Neutron Source Reactor*, ORNL/TM-12398, Martin Marietta Energy Systems, Inc., Oak Ridge Natl. Lab., May 1994, p. 4-1.

3. Ref. 2, p. 2–1.

4. Ref. 2, p. 4–4.

5. B. E. Foster, S. D. Snyder, and R. W. McClung, *Continuous Scanning X-Ray Attenuation Technique for Determining Fuel Inhomogeneities in Dispersion Core Fuel Plates*, ORNL-3737, Union Carbide Corp., Oak Ridge Natl. Lab., January 1965.

6. Ref. 2, p. 4–10.

7. "ORNL Homogeneity Scanner Control System Upgrade, Preliminary Design Specification," in *ORNL Homogeneity Scanner*, Babcock & Wilcox, Naval Nuclear Fuel Division, Lynchburg, Va., June 1992.

8. R. W. Knight, J. Binns, and G. M. Adamson, Jr., *Fabrication Procedures for Manufacturing High Flux Isotope Reactor Fuel Elements*, ORNL-4242, Union Carbide Corp., Oak Ridge Natl. Lab., June 1968, pp. 9–37.

9. Ref. 8, pp. 41–43.

10. Requests for approval and authorization from Texas Instruments, Inc. to G. M. Adamson, Union Carbide Corp., Nos. 391D (Feb. 19, 1973) 409D (Sept. 11, 1973), and 442D (Sept. 5, 1974).

11. I. Miller, J. Freund, and R. Johnson, *Probability and Statistics for Engineers*, 4th ed., Prentice-Hall, Inc., Englewood Cliffs, N. J., 1990.

12. Ref. 11, pp. 285 and 295.

APPENDIX A. DETERMINATION OF RELATIVE THICKNESS FOR USE IN OVERALL PERCENT DEVIATION CALCULATION

The overall percent deviation (PD) is a percentage expression of the measured mass of fuel in a fuel plate as compared with design specifications for fuel mass. The measured mass is calculated as a summation of the fuel masses contained in many small volumes within the fuel meat portion of the plate. These local masses are calculated as

$$m_{local} = \rho A_l \, th_{rel} \, th_{max} \quad , \tag{A1}$$

where

m_{local} = local mass,
ρ = nominal fuel density,
A_l = local area,
th_{rel} = relative thickness of the fuel meat at that location,
th_{max} = maximum thickness of the fuel meat.

The nominal density is available from fuel specifications. The local area is assumed to be a square region with sides as long as the distance between the homogeneity scan data points. The relative and maximum thicknesses can be found from design specifications after some additional calculations and considerations, which are presented here.

RELATIVE THICKNESS

The radial contour of the fuel meat thickness in HFIR fuel plates is specified in Fig.A.1. In this drawing, relative thickness is given as a function of radial position on the plate.

MAXIMUM THICKNESS

Maximum thickness can be found in two ways: from design dimensions as shown on Fig. A.1 or from manipulation of Eq. (5) and homogeneity scan data. Figure A.1 gives thickness dimensions for the various components of the fuel plate as well as total plate thickness. The maximum thickness calculated from these dimensions is 0.693 mm (0.027 in.).

A second way to calculate the maximum thickness is to assume that the oxide-loaded plate for which homogeneity scan data is available has an OPD of zero (i.e., measured total mass = specified total mass) and then to rearrange Eq. (5) as

$$th_{max} = \frac{\dfrac{OPD \times m_t}{100\%} + m_t}{A_l U_{loading} \times \sum \left[\left(\dfrac{PD}{100\%} + 1 \right) th_{rel} \right]} \, . \tag{A2}$$

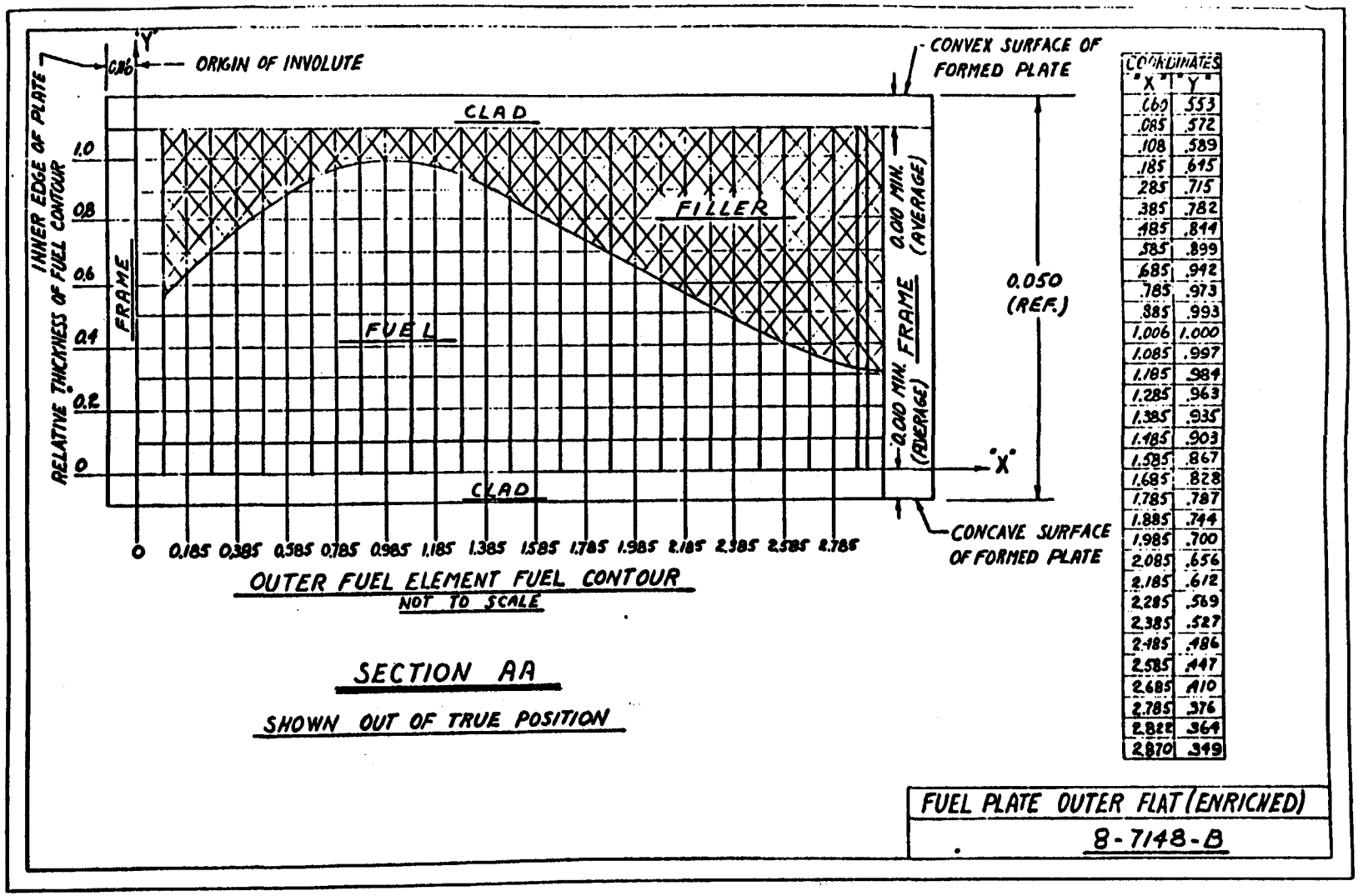

COORDINATES "X"	"Y"
.060	.553
.085	.572
.108	.589
.185	.615
.285	.715
.385	.782
.485	.844
.585	.899
.685	.942
.785	.973
.885	.993
1.006	1.000
1.085	.997
1.185	.984
1.285	.963
1.385	.935
1.485	.903
1.585	.867
1.685	.828
1.785	.787
1.885	.744
1.985	.700
2.085	.656
2.185	.612
2.285	.569
2.385	.527
2.485	.486
2.585	.447
2.685	.410
2.785	.376
2.828	.364
2.870	.349

Fig A.1. Radial contour of HFIR fuel plates. *Source*: Ref. 8.

The summation is then performed over the entire fueled region, with a value for the maximum thickness as a result. When this calculation was done for plate o195901, the resulting value was 0.694 mm (0.027 in.), which was in good agreement with the value derived from Fig. A.1, and was the value used in the OPD calculation of Eq. (5).

ALIGNING SCAN TRACKS WITH RADIAL LOCATION

To calculate nominal mass at a particular plate location, relative thickness must be known. Recall that the goal is to compare local masses represented by homogeneity scan data with nominal or design specified mass at the same location. To accomplish this, the locations represented by scan data must be matched with locations represented by design specifications. In Fig A.1., radial position is shown on the horizontal axis. In homogeneity scan data sets, radial position is given by track numbers. The challenge becomes to align scan track numbers with radial positions on Fig. A.1 and thus to obtain relative thickness as a function of track number. Since the distance between tracks is constant, it suffices to assign scan track 0 to a position on the horizontal axis of Fig. A.1.

The reference standards were used to perform this alignment. The reference standards represent a fuel plate with uniform fuel density; thus radial locations with identical thickness on the standard should generate identical counts values in the homogeneity scan data. Alignment of scan tracks with radial locations, then, can be checked by plotting counts values against relative thickness, beginning with an arbitrary assignment of track 0 to the radial position of 0.00 mm (0.00 in.) on Fig. A.1. Figure A.2 presents the resulting plot.

Because the same thickness values are traversed on either side of the fuel meat hump, a correct alignment should generate a plot with counts values that are the same on one side of the hump as on the other. If the alignment is incorrect, as in Fig. A.2, one thickness value will generate unequal counts values on either side of the fuel meat hump. Trial and error estimations, with this plot as a guide, led to a radial position of −1.19 mm (−0.047 in.) for track 0. This alignment resulted in the plot shown in Fig. A.3.

This method established the radial location of scan track 0. The relative thicknesses corresponding to the other scan tracks were then obtained by cubic interpolation between the data points used to create the plot shown in Fig. A.1. These relative thickness values were used in the OPD calculation of Eq. (5).

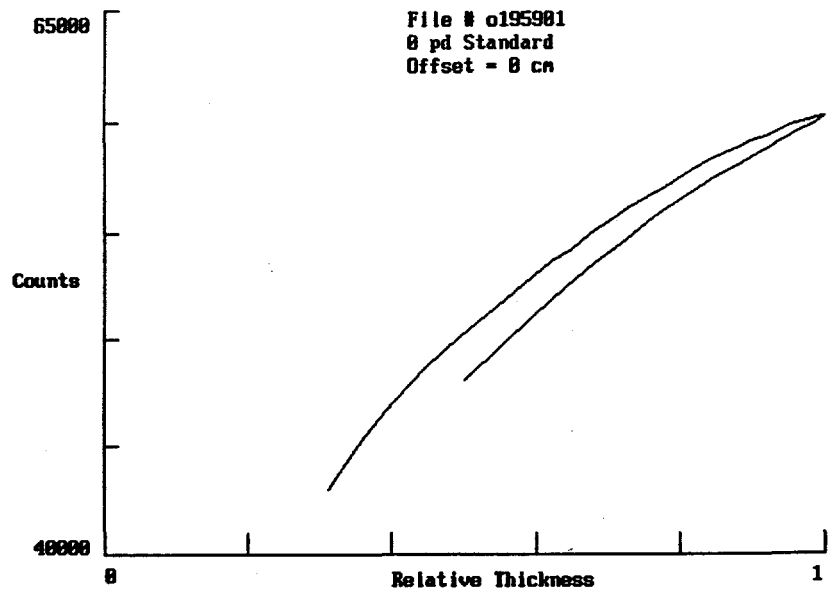

Fig. A.2. Counts vs relative thickness with track 0 set at 0.00 mm.

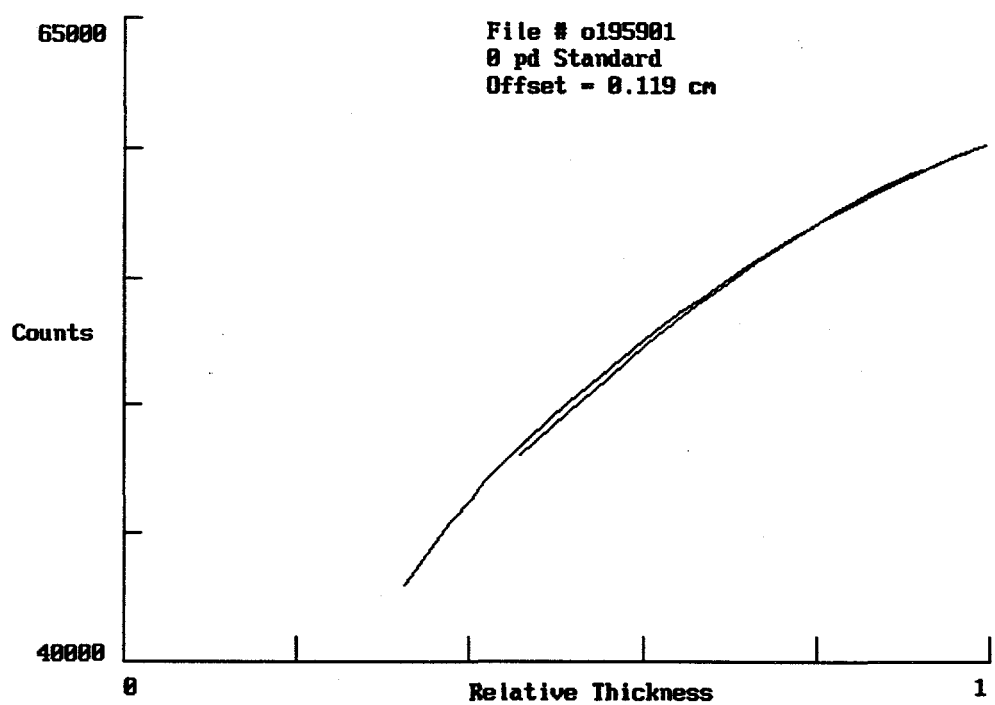

Fig. A.3. Counts vs relative thickness with track 0 set at –1.19 mm.

APPENDIX B. MANUFACTURING DATA FOR URANIUM SILICIDE LOADED FUEL PLATES

Quantity	Lot 7	Lot 8	Lot 9	HFIR outer
Fuel form	U_3Si_2	U_3Si_2	U_3Si_2	U308
Fuel lot	71902	71903	DEP-PP-001	521564
Fuel density, g/cc	12.21	12.19	11.95	8.24
U loading, g/cc	1.31	1.36	1.35	1.25
Al matrix	ALCAN 101	ALCAN 101	ALCAN 101	ALCAN 101
Al cladding	6061	6061	6061	6061
Fuel, g	23.43	23.34	23.18	23.45
Al matrix, g	37.50	37.51	37.44	35.00
Al filler, g	22.64	22.64	22.64	22.64

APPENDIX C. ASSUMPTIONS REQUIRED FOR OXIDE TO SILICIDE PERCENT DEVIATION CONVERSION

A downward shift in indicated percent deviation (PD) from nominal fuel loading was observed when testing plates loaded with silicide fuel against standards referenced to oxide fuel. When integrated across the entire fueled region of the plates, these reduced indicated loadings summed to overall fuel deficits in the plates. Because it is unlikely that all of the plates were actually loaded with less fuel than reported, a systematic measurement error was assumed responsible for the reduced indicated loadings. A correction scheme was derived from two basic assumptions. The derivation and application of the correction is presented in the body of the report; this appendix supports the assumptions underlying the correction scheme.

It was assumed that:

1. The plates contain the total reported fuel mass; i.e., there is no fuel missing. The overall percent deviation (OPD) is therefore an artifact of the measurement technique.
2. The OPD is constant over all locations in the fuel plate.

Assumption 1 is discussed above: the total mass within each plate is assumed to be the value reported on the data sheet in Appendix B as "Fuel, g." The remainder of this appendix is devoted to assumption 2.

Assumption 2 requires that the OPD have the same value when defined by integration over the entire plate as when defined locally at any location in the fueled region, *independent of fuel meat thickness*. To justify this assumption, a relationship between thicknesses for two different materials, incorporating a constant OPD, will be derived. This relationship will then be checked against available data to determine whether OPD is really a constant or whether it must be a function of thickness.

Begin by defining OPD as the PD between indicated masses (indicated by X-ray attenuation) for two materials:

$$OPD = \frac{m_1 - m_2}{m_2} \times 100\% \quad , \tag{C1}$$

where m_1 and m_2 are the masses of the two materials. For example, m_1 could be the total amount of fuel in a silicide plate *as indicated by oxide standards*, and m_2 could be the total amount of silicide fuel *known* (by assumption 1 *to be in a fuel plate*. By assumption 2, these masses may just as well be locally indicated masses at a single datum. Rearrange Eq. (C1):

$$\left(\frac{OPD}{100\%} + 1\right) m_2 = m_1 \quad . \tag{C2}$$

The local masses are

$$m_i = \rho_i A_i th_i \quad , \tag{C3}$$

where

m_i = either mass 1 or mass 2, ρ
ρ_i = the corresponding density (assumed constant),
A_i = the local area of the plate being examined (i.e., the "spot" area of the homogeneity scanner),
th_i= the local fuel meat thickness.

Substituting into the above and rearranging:

$$\frac{\left[\left(\frac{OPD}{100\%} + 1\right)\rho_2 A_l\right]}{\rho_1 A_l} \times th_2 = th_1 \quad . \tag{C4}$$

Thickness is known only as a function of attenuation, so the previous equation is expressed as a function of attenuation:

$$\frac{\left[\left(\frac{OPD}{100} + 1\right)\rho_2 A_l\right]}{\rho_1 A_l} \times th_2(\alpha_2) = th_1(\alpha_1) \quad , \tag{C5}$$

where α is the attenuation caused by material 1 or material 2. The functional form of the relationship between thickness and attenuation is not known analytically, so it is proposed to plot the locus of points on the (th_1, th_2) plane such that $\alpha_1 = \alpha_2$. The plot of this locus will be linear if OPD is truly independent of thickness.

Data from the homogeneity scanner relating thickness to attenuation (given constant, known density) are needed to generate the locus. Such data are not available for silicide fuel. These data are firmly established, however, for oxide fuel and for three materials that were considered for use as reference standards: 6061 T-6 aluminum, a 13% uranium-aluminum eutectic alloy, and tool steel.* Figure C.1 presents these data as the material thicknesses required to cause attenuations equal to those of known thicknesses of oxide fuel meat, thus forming three loci as proposed above.

On the plot, attenuation is indicated as "chart" reading (referring to the chart recorder used for analog data acquisition in the homogeneity scanner). The oxide fuel meat thickness was calculated from the original data for areal uranium loading by use of a form of Eq. (C3) and density data from Appendix B.

The linear nature of the loci in Fig. C.1 indicates that Eq. (C5) is valid for the materials examined and that, for these materials, OPD is indeed independent of thickness. Further, an extrapolation of the locus for aluminum intercepts the y-axis at a thickness just slightly greater than the total thickness of a fuel plate. This is an excellent model of physical reality: as fuel meat becomes thinner in a fuel plate, constant plate thickness is maintained with aluminum powder. In the limit of zero fuel meat thickness, the aluminum thickness would be the total plate thickness. It may be that the slight error results from a difference in aluminum density and composition: plates are filled with powdered "pure" aluminum, not homogeneous 6061 alloy.

*Ref. 5, Figs. 5, 7, and 8.

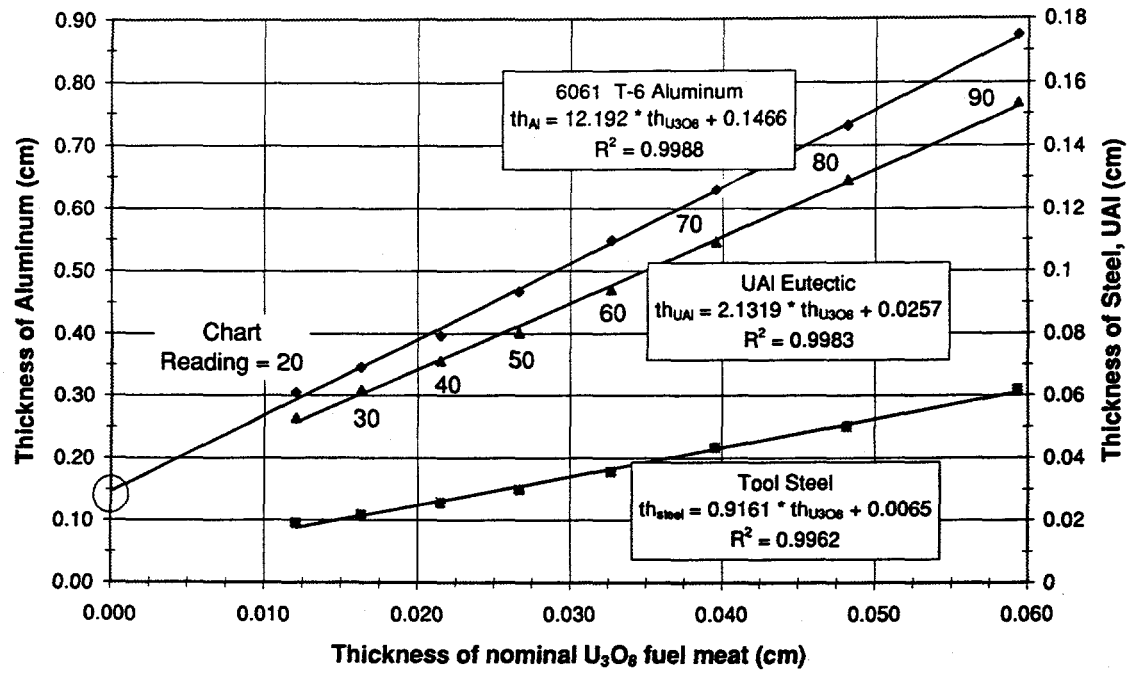

Fig. C.1. Material thickness correlations for equal attenuations.

It is now hypothesized that the locus of silicide fuel meat thicknesses for equal attenuation with oxide fuel meat thickness will also be linear. Against this hypothesis, it has been suggested that differences in particle size parameters between the two materials will lead to nonlinearities in the relationship between oxide and silicide attenuation. There are, however, much greater differences in material composition between particulate oxide fuel and the three homogeneous metals analyzed in Fig. C.1 than there are between oxide and silicide fuel. It is therefore believed that if particle parameter effects were significant, they would be made manifest as nonlinearities in Fig. C.2.

The justification of assumption 2 rests on the validity of the above hypothesis, which must remain unproven until data have been collected for attenuation in silicide fuel, as they were for oxide fuel and the other materials. When attenuation data for silicide fuel become available, they are predicted to fall along the hypothetical locus generated in Fig. C.2. This figure presents data for equal attenuation in oxide fuel and aluminum and a hypothetical locus for silicide fuel and aluminum, assuming an OPD of −10.5% (representative of fuel lot 900). Note that the predicted behavior for the silicide fuel maintains the desired boundary condition of attenuation equivalent to an all-aluminum plate in the limit of zero fuel meat thickness.

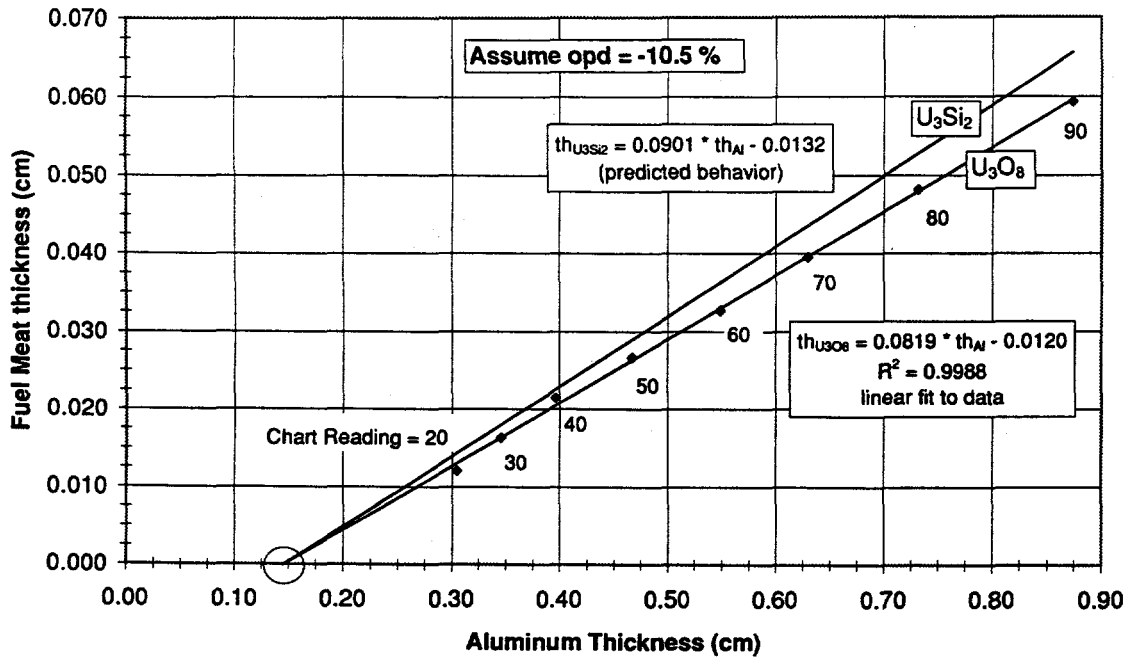

Fig. C.2. Observed U_30_8 and hypothetical U_3Si_2 fuel meat thickness correlated with aluminum thickness.

INTERNAL DISTRIBUTION

1–5. P. E. Blumenfeld
6–7. J. H. Campbell
8. D. H. Cook
9. G. L. Copeland
10. W. G. Craddick
11. G. F. Flanagan
12–15. R. L. Johnson
16. R. W. Knight
17. D. G. Morris
18. R. B. Rothrock
19. J. D. Sease
20. D. L. Selby
21. M. Siman-Tov
22. C. D. West
23. G. L. Yoder
24. ORNL Patent Office
25. Central Research Library Document Reference Section
26. Y-12 Technical Library
27–28. Laboratory Record Dept.
29. Laboratory Records, RC

EXTERNAL DISTRIBUTION

30. J. E. Mays, Research and Test Reactor Fuel Elements, Babcock and Wilcox Co., P.O. Box 785, Lynchburg, VA 24505.
31. J. L. Snelgrove, Coordinator, Engineering Applications, REPTR Program, Argonne National Laboratory, 9700 South Cass Ave., Argonne, IL 60439
32. U.S. Department of Energy, ANS Project Office, Oak Ridge Operations Office, FEDC, MS-8218, P.O. Box 2009, Oak Ridge, TN 37831-8218.
33–34. Office of Scientific and Technical Information, P.O. Box 63, Oak Ridge, TN 37831.